

October 1999

Modifications of the Rho Meson from the Virtual Pion Cloud in Hot and Dense Matter

M. Urban, M. Buballa and J. Wambach

Institut für Kernphysik, TU Darmstadt, Schlossgartenstr. 9, 64289 Darmstadt, Germany

Abstract

The modification of the ρ -meson self-energy due to the coupling to in-medium pions is calculated consistently at finite baryon density and temperature, keeping the full 3-momentum dependence in a gauge invariant way. At low energies a strong increase of the imaginary part is found as a combined effect of temperature and baryon density. However, for energies above ≈ 300 MeV the medium modifications are mainly due to density effects. While, at a given baryon density, the ρ -meson width remains almost unchanged as a function of temperature, the pole mass is slightly shifted upwards. As a consequence, the resulting production rates for dileptons and real photons are somewhat reduced as compared to those obtained by neglecting temperature effects.

1 Introduction

In the last few years the spectra of dilepton pairs (e^+e^- or $\mu^+\mu^-$) emerging from (ultra-) relativistic heavy-ion collisions have been measured in various experiments. Despite of low production rates, resulting in large statistical errors, dileptons have the distinct advantage to reach the detector almost undisturbed and are therefore in principle ideal probes for studying the hot and dense initial phases of the fireball [1]. Strongly interacting particles on the other hand undergo many collisions, such that they finally carry only information about the freeze-out conditions.

The dilepton production rate in a hot and dense medium is directly related to the electromagnetic current-current correlation function. In the hadronic phase of the fireball and in the low invariant-mass region, $M \lesssim 1$ GeV (M = invariant mass of the dilepton pair), this correlation function is largely saturated by the ρ -, ω - and ϕ -mesons through vector meson dominance [2, 3]. Hence dilepton spectra contain information about the properties (mass, width) of these mesons in the surrounding medium, most prominently the ρ meson due to its large dilepton decay width (see [4] for a recent review).

From a field theoretical point of view, the modifications of the ρ -meson properties are described by its self-energy Σ , which contains all interactions with the surrounding matter. In vacuum the ρ -meson receives a width of ≈ 150 MeV from the decay into two pions, corresponding to the self-energy diagram $\Sigma_{\rho\pi\pi}$, shown in Fig. 1a. In cold nuclear matter pions are strongly modified by Delta-hole (Δh) excitations as evidenced from the wealth of pion-nucleus data [5]. It is therefore suggestive to include medium modifications by replacing the free pions in $\Sigma_{\rho\pi\pi}$, by in-medium ones [6, 7, 8, 9]. Of course the ρ -meson can also interact resonantly with the nucleons as described by the self-energy contributions shown in Fig. 1b and denoted by $\Sigma_{\rho B}$ [10, 11]. At finite temperature self-energy contributions $\Sigma_{\rho M}$, such as the one shown in Fig. 1c describing direct interactions with thermal mesons, need to be considered in addition. Combining these three self-energy contributions, $\Sigma = \Sigma_{\rho\pi\pi} + \Sigma_{\rho B} + \Sigma_{\rho M}$, a reasonable description of the dilepton spectra measured by the CERES collaboration [12] can be achieved [13, 14]. In this description the ρ -meson acquires a substantial width and ceases to be a well-defined quasiparticle [4].

In the present article we will restrict ourselves to the contribution $\Sigma_{\rho\pi\pi}$, which is probably the most difficult part. In the first calculations of $\Sigma_{\rho\pi\pi}$ in matter, the flat

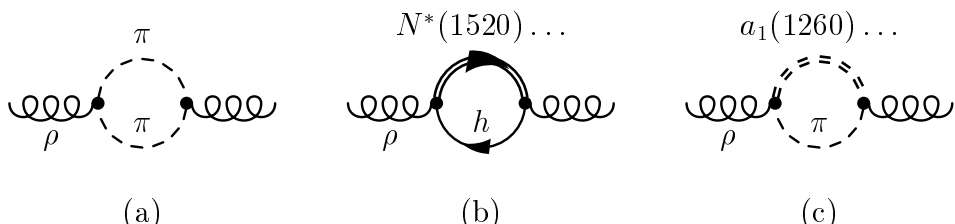


Figure 1: Examples for different contributions to the ρ -meson self-energy in hadronic matter: (a) Decay into two pions, $\Sigma_{\rho\pi\pi}$. (b) Excitation of baryonic resonances via ρN scattering in baryon rich matter, $\Sigma_{\rho B}$. (c) Excitation of mesonic resonances in $\rho\pi$ scattering in a hot meson gas, $\Sigma_{\rho M}$.

dispersion relation of the in-medium pions produced a divergence of $\Sigma_{\rho\pi\pi}$ near the two pion threshold [6]. However, gauge invariance was violated in these calculations. To correct this, appropriate $\rho\pi\pi$ vertex corrections had to be included, which canceled the divergence [7, 8, 9]. Chanfray and Schuck [8] and Herrmann et al. [9] restricted themselves to ρ -mesons at rest and zero temperature. In Ref. [15] we presented an extension of their models to ρ -mesons in cold nuclear matter with finite 3-momentum. When applied to photoabsorption cross sections for nucleons and nuclei [16], it was found that the pion-nucleon and pion-Delta form factors had to be chosen rather soft, resulting in reduced in-medium contributions from $\Sigma_{\rho\pi\pi}$.

For a consistent calculation of dilepton rates it is important to include also temperature. This is the aim of the present article. We start with a brief description of our model for $\Sigma_{\rho\pi\pi}$ (in the following denoted Σ for simplicity) without baryons, i.e. in vacuum or in a hot meson gas. Section 3 discusses the medium modifications of the pion propagator in hot baryon rich matter, which will be used in Section 4 to calculate Σ at finite temperature and baryon density. The combined effects of temperature and baryon density on dilepton and photon rates are studied in Section 5.

2 The ρ -meson in a hot pion gas

Before taking into account baryonic effects, we briefly discuss the ρ -meson self-energy at zero baryon density, $\varrho_B = 0$, i.e. in vacuum (temperature $T = 0$) and in a hot pion gas (temperature $T > 0$). Minimal substitution leads to the following $\pi\rho$ interaction Lagrangian [9]:

$$\mathcal{L}_{\pi\rho} = \frac{1}{2}ig\rho_\mu(T_3\vec{\phi} \cdot \partial^\mu\vec{\phi} + \partial^\mu\vec{\phi} \cdot T_3\vec{\phi}) - \frac{1}{2}g^2\rho_\mu\rho^\mu T_3\vec{\phi} \cdot T_3\vec{\phi}, \quad (1)$$

where $\vec{\phi}$ denotes the isovector pion field, ρ_μ the field of the neutral ρ -meson, T_3 the third component of the isospin operator and g the $\rho\pi\pi$ coupling constant. The ρ -meson self-energy to order g^2 is represented by the two diagrams shown in Figs. 2a and 2b. Calculating these diagrams within the imaginary-time formalism described

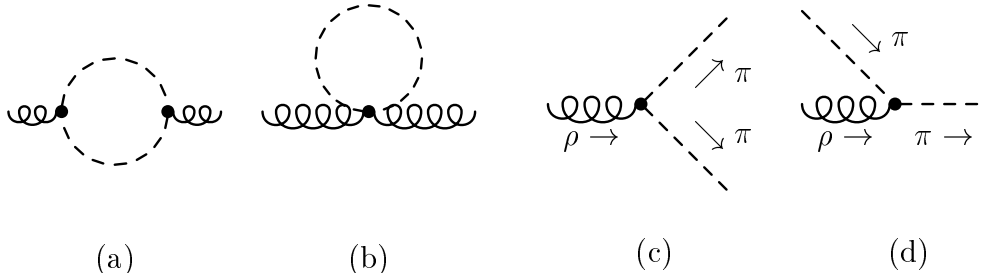


Figure 2: (a) and (b) Diagrams for the ρ -meson self-energy at zero baryon density. (c) and (d) Processes contributing to the imaginary part of diagram (a) at finite temperature $T > 0$: (c) $\rho \rightarrow \pi + \pi$ (decay of a ρ -meson into two pions), (d) $\rho + \pi \rightarrow \pi$ (absorption of a virtual ρ -meson by a thermal pion).

e.g. in Ref. [17], we finally obtain the following expression for the spatial components ($i, j = 1, 2, 3$) of the retarded ρ -meson self-energy tensor $\Sigma_{\mu\nu}$ (see Section 4 for details):

$$\begin{aligned} \Sigma_{ij}(q_0, \vec{q}) = & g^2 \int \frac{d^3 k}{(2\pi)^3} (2k + q)_i (2k + q)_j \left(\frac{(1 + 2n_{\vec{k}})(\omega_{\vec{k}+\vec{q}} + \omega_{\vec{k}})}{2\omega_{\vec{k}+\vec{q}}\omega_{\vec{k}}((q_0 + i\varepsilon)^2 - (\omega_{\vec{k}+\vec{q}} + \omega_{\vec{k}})^2)} \right. \\ & \left. + \frac{n_{\vec{k}}(\omega_{\vec{k}+\vec{q}} - \omega_{\vec{k}})}{\omega_{\vec{k}+\vec{q}}\omega_{\vec{k}}((q_0 + i\varepsilon)^2 - (\omega_{\vec{k}+\vec{q}} - \omega_{\vec{k}})^2)} \right) \\ & + g^2 \delta_{ij} \int \frac{d^3 k}{(2\pi)^3} \frac{1 + 2n_{\vec{k}}}{\omega_{\vec{k}}}. \end{aligned} \quad (2)$$

Here we have used the short-hand notation $\omega_{\vec{k}} = \sqrt{m_\pi^2 + \vec{k}^2}$ and $n_{\vec{k}} = 1/(e^{\omega_{\vec{k}}/T} - 1)$.

The self-energy Σ can be separated into vacuum and medium contributions, $\Sigma = \Sigma^{vac} + \Sigma^{med}$ (terms $\propto 1$ and $\propto n_{\vec{k}}$, respectively). In order to preserve current conservation and Lorentz invariance in the vacuum, the divergent integrals in Σ^{vac} are regularized using the Pauli-Villars scheme. The free parameters of the model (bare ρ mass $m_\rho^{(0)} = 853$ MeV, coupling constant $g = 5.9$ and Pauli-Villars regulator mass $\Lambda_\rho = 1$ GeV) are adjusted such that the electromagnetic form factor of the pion and the $\pi\pi$ scattering phase shifts δ_1^1 are reproduced satisfactorily (see Ref. [15] for details). Numerical results for $\text{Im } \Sigma^{vac}$, $\text{Re } \Sigma^{vac}$ and the ρ -meson spectral function in vacuum $-\text{Im } G_\rho^{vac}$ are displayed in Fig. 3 as the dotted lines.

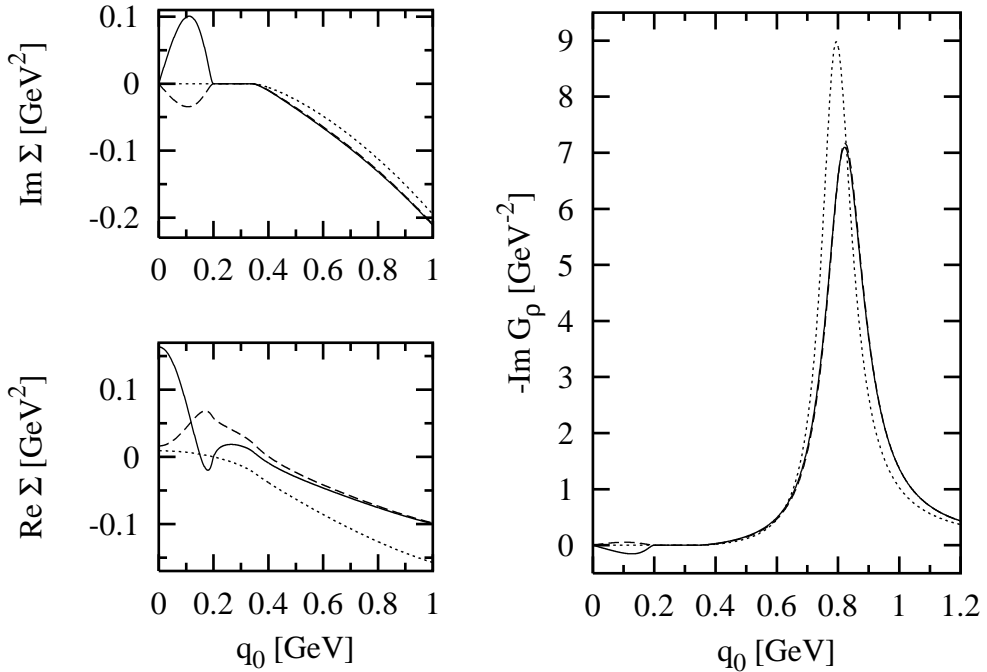


Figure 3: (Left panel) Real and imaginary part of the ρ -meson self-energy at $\varrho_B = 0$ for fixed $|\vec{q}| = 200$ MeV as a function of q_0 at $T = 0$ (Σ^{vac} , dotted lines) and $T = 150$ MeV (Σ_T , dashed lines, and Σ_L , solid lines). (Right panel) Corresponding ρ -meson spectral functions $-\text{Im } G_\rho^{vac}$, $-\text{Im } G_\rho T$ and $-\text{Im } G_\rho L$.

Let us now discuss the medium contribution Σ^{med} . As there exists a preferred frame of reference in the heat bath, Σ depends on q_0 and \vec{q} separately, and splits into 3-dimensionally transverse and longitudinal parts Σ_T and Σ_L [18], which are related to the spatial components of the self-energy tensor by

$$\Sigma_T = \frac{1}{2} \left(\delta^{ij} - \frac{q^i q^j}{\vec{q}^2} \right) \Sigma_{ij} , \quad \Sigma_L = \frac{q^2}{q_0^2} \frac{q^i q^j}{\vec{q}^2} \Sigma_{ij} . \quad (3)$$

(In the special case $\vec{q} = 0$ this reduces to $\Sigma_T = \Sigma_L = \frac{1}{3} \delta^{ij} \Sigma_{ij}$.) The angular integrations for Σ_T^{med} and Σ_L^{med} can be performed analytically. For time-like momenta, $q^2 > 0$, the final expressions are given e.g. in Ref. [18]. Numerical results for Σ_T and Σ_L as well as the corresponding ρ -meson spectral functions $-\text{Im } G_{\rho T}$ and $-\text{Im } G_{\rho L}$ are shown in Fig. 3 for fixed 3-momentum $|\vec{q}| = 200$ MeV as a function of q_0 . Above the two-pion threshold, $q^2 > 4m_\pi^2$, i.e. $q_0 > 344$ MeV in Fig. 3, the ρ -meson self-energy receives an imaginary part from the first term in Eq. (2), which describes the decay into a $\pi^+ \pi^-$ pair (Fig. 2c). This imaginary part exists already in vacuum, but is Bose-enhanced by a factor $1 + 2n_{\vec{k}}$ at $T > 0$. In the space-like region, $q^2 < 0$, i.e. $q_0 < 200$ MeV in Fig. 3, also the second term in Eq. (2) generates an imaginary part in Σ_T and Σ_L , describing the absorption of the virtual ρ -meson by a thermal pion (Fig. 2d) and therefore vanishing in vacuum. The main reason for the completely different behavior of Σ_T and Σ_L in this region is the factor q^2/q_0^2 in Eq. (3). The real parts of Σ_T and Σ_L near the ρ -meson pole are larger than the real part of Σ^{vac} , thus shifting the pole to higher energies. This and the broadening due to the factor $1 + 2n_{\vec{k}}$ in $\text{Im } \Sigma$ can be seen in the ρ -meson spectral function (right panel of Fig 3).

3 The pion in hot nuclear matter

In cold nuclear matter the interaction of the pion with the surrounding nucleons leads to a mixture of the pion with particle-hole (Nh) and Delta-hole (Δh) excitations. In this section we will evaluate the corresponding diagrams at finite temperature T . As in our zero temperature calculation [15], we start from the interaction Lagrangians

$$\mathcal{L}_{\pi N} = \frac{f_{\pi NN}}{m_\pi} \bar{\psi} \gamma^5 \gamma^\mu \vec{\tau} \psi \cdot \partial_\mu \vec{\phi} , \quad \mathcal{L}_{\pi N \Delta} = -\frac{f_{\pi N \Delta}}{m_\pi} \bar{\psi} \vec{\tau}^\dagger \psi_\mu \cdot \partial^\mu \vec{\phi} + \text{h.c.} , \quad (4)$$

with $f_{\pi NN}^2/(4\pi) = 0.081$ and $f_{\pi N \Delta} = 2f_{\pi NN}$ (Chew-Low value), and expand the vertices and spinors to leading order in $1/m_N$ or $1/m_\Delta$ to obtain standard non-relativistic Feynman rules. In the nucleon and Delta propagators, we neglect the antiparticle contributions, but keep the relativistic kinematics, $\omega_{N,\Delta}(\vec{p}) = \sqrt{m_{N,\Delta}^2 + \vec{p}^2}$. (We have performed the calculations also with the non-relativistic kinematics, $\omega_{N,\Delta}(\vec{p}) = m_{N,\Delta} + \vec{p}^2/(2m_{N,\Delta})$, and found only very small differences in the final results for the ρ -meson self-energy.)

Now, calculating Nh and Δh excitations at finite temperature, we obtain the following generalized Lindhard functions:

$$\Pi_{Nh}(k_0, \vec{k}) = 4 \left(\frac{f_{\pi NN}}{m_\pi} \right)^2 \int \frac{d^3 p}{(2\pi)^3} n_N(\vec{p}) \frac{2(\omega_N(\vec{p} + \vec{k}) - \omega_N(\vec{p}))}{(k_0 + i\varepsilon)^2 - (\omega_N(\vec{p} + \vec{k}) - \omega_N(\vec{p}))^2} , \quad (5)$$

$$\begin{aligned}
\Pi_{\Delta h}(k_0, \vec{k}) &= \frac{16}{9} \left(\frac{f_{\pi N \Delta}}{m_\pi} \right)^2 \int \frac{d^3 p}{(2\pi)^3} (n_N(\vec{p}) - n_\Delta(\vec{p} + \vec{k})) \\
&\quad \times \frac{2(\omega_\Delta(\vec{p} + \vec{k}) - \omega_N(\vec{p}))}{(k_0 + \frac{i}{2}\Gamma_\Delta)^2 - (\omega_\Delta(\vec{p} + \vec{k}) - \omega_N(\vec{p}))^2} . \quad (6)
\end{aligned}$$

Here we have adopted the notation $n_{N,\Delta}(\vec{p}) = 1/(e^{(\omega_{N,\Delta}(\vec{p}) - \mu_B)/T} + 1)$, where the baryon chemical potential μ_B as a function of ϱ_B and T is determined by

$$\varrho_B = \varrho_N + \varrho_\Delta , \quad \varrho_N = 4 \int \frac{d^3 p}{(2\pi)^3} n_N(\vec{p}) , \quad \varrho_\Delta = 16 \int \frac{d^3 p}{(2\pi)^3} n_\Delta(\vec{p}) , \quad (7)$$

i.e. in this context the Delta is treated as a stable particle. However, in the Δh Lindhard function $\Pi_{\Delta h}$ (Eq. (6)), a constant Delta width Γ_Δ is introduced, in such a way that $\Pi_{\Delta h}$ has the analytic properties of a Fourier transformed retarded function.

As described in Ref. [15], we account for the effect of the repulsive short-range NN and $N\Delta$ interaction through phenomenological Migdal parameters g' [19], which is important to avoid pion condensation. The fact that nucleon and Delta are not elementary particles is taken into account by introducing a monopole form factor $\Gamma_\pi(\vec{k}) = \Lambda^2/(\Lambda^2 + \vec{k}^2)$ at the πNN and $\pi N\Delta$ vertices. The values of the parameters g' and Λ are obtained from a fit to photoabsorption cross sections [15, 16] resulting in: $g'_{11} = 0.6$, $g'_{12} = g'_{22} = 0.25$ and $\Lambda = 550$ MeV. Now the total pion self-energy reads

$$\Pi = \Gamma_\pi^2 \frac{\Pi_{Nh} + \Pi_{\Delta h} - (g'_{11} - 2g'_{12} + g'_{22})\Pi_{Nh}\Pi_{\Delta h}}{1 - g'_{11}\Pi_{Nh} - g'_{22}\Pi_{\Delta h} + (g'_{11}g'_{22} - g'_{12}^2)\Pi_{Nh}\Pi_{\Delta h}} , \quad (8)$$

and the in-medium pion propagator is given by

$$G_\pi(k_0, \vec{k}) = \frac{1}{(k_0 + i\varepsilon)^2 - m_\pi^2 - \vec{k}^2(1 + \Pi(k_0, \vec{k}))} . \quad (9)$$

The influence of temperature on the medium modifications can be summarized as follows: For fixed baryon density ϱ_B the nucleon density ϱ_N becomes smaller at finite temperature T according to Eq. (7). This reduces the strength of Nh and Δh excitations. Furthermore, as also Delta states are occupied, Δh excitations become suppressed by Pauli blocking¹. Another temperature effect is the broadening of the Nh and Δh Lindhard functions due to thermal motion of the nucleons and Deltas. The peaked structures in the pion spectral function (Nh , π and Δh peaks), which exist at zero temperature, become completely washed out at higher temperatures as indicated in Fig. 4.

At zero temperature the in-medium pion can be described as a mixture of three quasi-particles, $(Nh)_L$, π and $(\Delta h)_L$. This so-called “three-level model” is equivalent to neglecting the Fermi motion of the nucleons. As a consequence of the temperature effects described above, it seems to be not very reasonable to construct such a model also for $T > 0$.

¹In reality these two effects might be less important, because the role of the suppressed $Nh = NN^{-1}$ and $\Delta h = \Delta N^{-1}$ excitations might be taken over by $B_1^* B_1^{*-1}$ and $B_2^* B_1^{*-1}$ excitations [14], where B_1^* and B_2^* denote any baryon resonances ($\Delta(1232)$, $N^*(1520)$ etc.). Unfortunately most of the $\pi B_1^* B_1^*$ and $\pi B_1^* B_2^*$ coupling constants are not known.

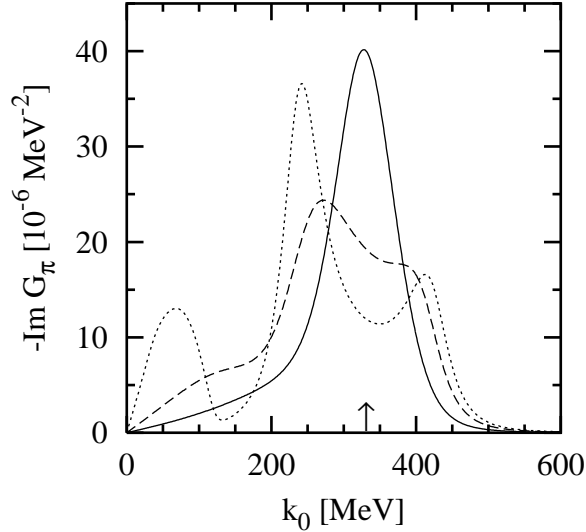


Figure 4: Imaginary part of the in-medium pion propagator for fixed 3-momentum $|\vec{k}| = 300$ MeV as a function of energy k_0 , for nuclear matter saturation density $\varrho_B = \varrho_0 = 0.16 \text{ fm}^{-3}$ and various temperatures: $T = 0$ (dotted line), $T = 80$ MeV (dashed line), $T = 150$ MeV (solid line). For comparison, the arrow indicates the pole position of a free pion ($k_0 \approx 331$ MeV).

4 The ρ -meson self-energy in hot nuclear matter

It has been shown by several authors [7, 8, 9], that simply replacing the free pion propagators in the ρ -meson self-energy (Figs. 2a and 2b) by in-medium ones violates gauge invariance and leads to a strong overestimation of the medium modifications. To preserve gauge invariance, corrections to the $\rho\pi\pi$ and $\rho\rho\pi\pi$ vertices must be taken into account, which are related to the pion self-energy through Ward-Takahashi identities. For illustration, some of the vertex corrections related to the Nh pion self-energy contribution are shown in Fig. 5. Neglecting the anomalous magnetic moments of the nucleons, the ρNN and $\rho\pi NN$ couplings can be derived by minimal substitution in the free nucleon

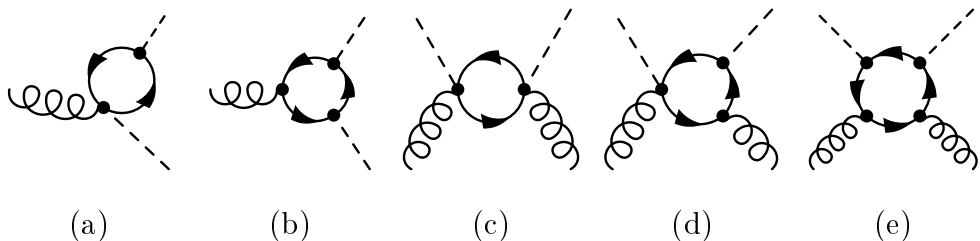


Figure 5: Some of the $\rho\pi\pi$ and $\rho\rho\pi\pi$ vertex correction diagrams corresponding to the Nh pion self-energy.

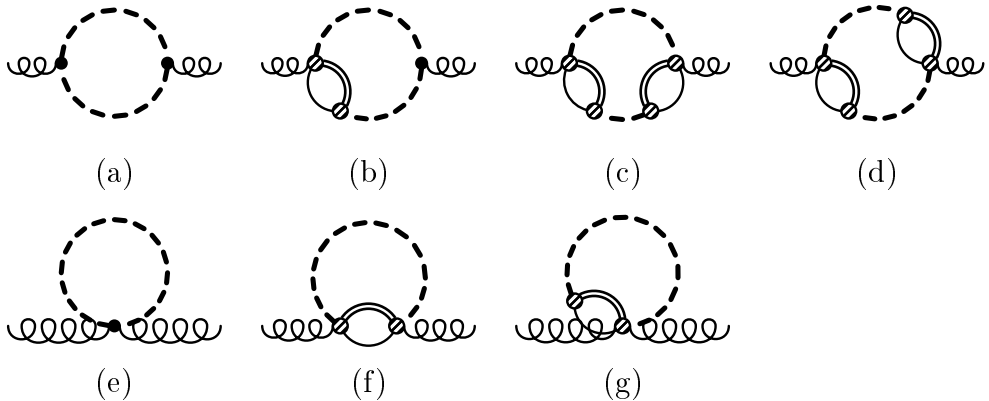


Figure 6: Feynman diagrams for the spatial components of the pion cloud contribution to the ρ -meson self-energy in hot hadronic matter. The thick dashed lines represent in-medium pion propagators, the bubbles represent the total pion self-energy with the πNN or $\pi N\Delta$ monopole form factors indicated by the hatched blobs.

Lagrangian \mathcal{L}_N and the πN interaction Lagrangian $\mathcal{L}_{\pi N}$:

$$\mathcal{L}_{\rho N} = -\frac{g}{2}\bar{\psi}\not{\rho}\tau_3\psi, \quad \mathcal{L}_{\rho\pi N} = ig\frac{f_{\pi NN}}{m_\pi}\bar{\psi}\gamma^5\not{\rho}\vec{\tau}\psi \cdot T_3\vec{\phi}. \quad (10)$$

In Ref. [15] we have shown that the leading term in a non-relativistic expansion of the ρNN interaction is the coupling of the ρ -meson to the nucleon charge, contributing only to the time component of the ρNN vertex. The spatial components are of the order $1/m_N$. If we neglect them, only the diagrams shown in Figs. 5a and 5c are relevant for the spatial components of the ρ -meson self-energy². For the Δh part, similar vertex corrections must be calculated. This can be done in analogy to the $N h$ part described above. The Migdal parameters g' correspond to an iteration of the $N h$ and Δh bubbles and therefore lead to additional vertex corrections. Because of the monopole form factor Γ_π at the πNN and $\pi N\Delta$ vertices, the $\rho\pi NN$ and $\rho\pi N\Delta$ vertices must be modified in a non-trivial way [9, 20] as has been described in detail in Ref. [15].

With these vertex corrections the spatial components Σ_{ij} of the ρ -meson self-energy become a sum of seven terms, corresponding to the seven classes of diagrams shown in Fig. 6. The diagrams 6a and 6e are the same as in vacuum (Figs. 2a and 2b), but with the bare pion propagators replaced by in-medium ones. The diagrams 6b to 6d and 6f to 6g are obtained by including $\rho\pi\pi$ vertex corrections in diagram 6a and $\rho\rho\pi\pi$ vertex corrections in diagram 6d, respectively. The diagrams 6a to 6d and 6f can be cut into two parts, i.e. they depend on q_0 and \vec{q} and contribute to both the real and imaginary parts of Σ_{ij} . The diagrams 6e and 6g cannot be cut and are therefore real and q_0 -independent.

²Within a slightly simplified model (zero temperature, 2-level model for the pion without Migdal parameter g'), we have performed the full calculation also allowing for ρ -meson coupling to the convection current. For time-like momenta, $q^2 > 0$, which are relevant for dilepton spectra, the effect of these terms is small, but, as expected, in the space-like region near the quasi-elastic peak, the approximation becomes quite bad.

However, because of the coupling of the ρ -meson to the πNN and $\pi N\Delta$ monopole form factor in diagram 6g, their contribution still depends on the 3-momentum \vec{q} .

Let us first look at these purely real and energy independent (“constant”) contributions. Their sum, Σ_{ij}^C , has the structure

$$\Sigma_{ij}^C(\vec{q}) = g^2 \int \frac{d^3 k}{(2\pi)^3} \sum_{r=5,7} f_{ij}^{(r)}(\vec{q}, \vec{k}) J_r(\vec{k}) . \quad (11)$$

The $r = 5$ and $r = 7$ terms correspond to the diagrams 6e and 6g, respectively. Explicit expressions for the functions $f_{ij}^{(r)}$, which are simple combinations of \vec{q} , \vec{k} and Λ , are given in the appendix. The functions J_5 and J_7 are defined as sums over Matsubara frequencies $\omega_m = \pi m T$:

$$J_5(\vec{k}) = -2T \sum_{m \text{ even}} \mathcal{G}_\pi(\omega_m, \vec{k}) , \quad J_7(\vec{k}) = -2T \sum_{m \text{ even}} \Pi(\omega_m, \vec{k}) \mathcal{G}_\pi(\omega_m, \vec{k}) . \quad (12)$$

Here $\mathcal{G}_\pi(\omega_m, \vec{k})$ denotes the imaginary-time pion propagator, which is related to the retarded propagator G_π by its Lehmann representation [17],

$$\mathcal{G}_\pi(\omega_m, \vec{k}) = -\frac{1}{\pi} \int d\omega \frac{\text{Im } G_\pi(\omega, \vec{k})}{i\omega_m - \omega} . \quad (13)$$

In an analogous way $\Pi(\omega_m, \vec{k})$ is related to the retarded pion self-energy Π . Inserting this into Eq. (12) and using the identity

$$-T \lim_{\eta \rightarrow 0} \sum_{m \text{ even}} \frac{e^{i\omega_m \eta}}{i\omega_m - \omega} = \frac{1}{e^{\omega/T} - 1} =: f(\omega) , \quad (14)$$

we can evaluate the sum over ω_m , with the result

$$J_5(\vec{k}) = -\frac{2}{\pi} \int_0^\infty d\omega \left(1 + 2f(\omega) \right) \text{Im } G_\pi(\omega, \vec{k}) \quad (15)$$

and a similar expression for J_7 .

Next we turn to the energy dependent part of Σ_{ij} , represented by the diagrams 6a to 6d and 6f. It has the structure

$$\Sigma_{ij}(q_0, \vec{q}) - \Sigma_{ij}^C(\vec{q}) = g^2 \int \frac{d^3 k}{(2\pi)^3} \sum_{r=1,2,3,4,6} f_{ij}^{(r)}(\vec{q}, \vec{k}) I_r(q_0, \vec{q}, \vec{k}) . \quad (16)$$

The $r = 1$, $r = 2$ and $r = 4$ terms correspond directly to the diagrams 6a, 6b and 6d, whereas the definitions of the $r = 3$ and $r = 6$ terms are somewhat more complicated: The pion self-energy bubble in diagram 6f can be separated into a spin-longitudinal and a spin-transverse part. The $r = 6$ term contains only the transverse part, whereas the longitudinal part is combined with diagram 6c in the $r = 3$ term.

Note that the entire q_0 dependence is contained in the functions I_r . These are obtained by analytical continuation of functions J_r , which originally are defined only for discrete Matsubara frequencies ω_n , n even:

$$I_r(q_0, \vec{q}, \vec{k}) = J_r(\omega_n \rightarrow -i(q_0 + i\varepsilon), \vec{q}, \vec{k}) . \quad (17)$$

For example, the function J_1 is defined as follows:

$$J_1(\omega_n, \vec{q}, \vec{k}) = -2T \sum_{m \text{ even}} \mathcal{G}_\pi(\omega_m, \vec{k}) \mathcal{G}_\pi(\omega_{m+n}, \vec{k} + \vec{q}) . \quad (18)$$

The definitions of the other functions J_r are listed in the appendix.

As described already for J_5 , we insert the Lehmann representation of \mathcal{G}_π into Eq. (18) and evaluate the sum over ω_m by using Eq. (14). After these steps the analytical continuation of J_1 to I_1 reduces to a simple replacement according to Eq. (17). For the imaginary part we obtain

$$\begin{aligned} \text{Im } I_1(q_0, \vec{q}, \vec{k}) = & -\frac{2}{\pi} \int_0^{q_0} d\omega \left(1 + f(\omega) + f(q_0 - \omega) \right) \\ & \times \text{Im } G_\pi(\omega, \vec{k}) \text{Im } G_\pi(q_0 - \omega, \vec{k} + \vec{q}) \\ & -\frac{2}{\pi} \int_0^\infty d\omega \left(f(\omega) - f(q_0 + \omega) \right) \\ & \times \left(\text{Im } G_\pi(\omega, \vec{k}) \text{Im } G_\pi(q_0 + \omega, \vec{k} + \vec{q}) \right. \\ & \left. + \text{Im } G_\pi(q_0 + \omega, \vec{k}) \text{Im } G_\pi(\omega, \vec{k} + \vec{q}) \right) . \end{aligned} \quad (19)$$

In the same way we derive similar expressions for the imaginary parts of the remaining functions I_2 to I_4 and I_6 . Rather than by direct calculation, the real part of the energy-dependent part of the ρ -meson self-energy, $\Sigma_{ij} - \Sigma_{ij}^C$, can be computed more efficiently from the imaginary part using a dispersion relation. The convergence of the dispersion integral is improved by subtracting the vacuum contribution:

$$\text{Re } \Sigma_{ij}^{med}(q_0, \vec{q}) - \Sigma_{ij}^{C \text{ med}}(\vec{q}) = -\frac{1}{\pi} \mathcal{P} \int_0^\infty d\omega^2 \frac{\text{Im } \Sigma_{ij}^{med}(\omega, \vec{q})}{q_0^2 - \omega^2} . \quad (20)$$

In Fig. 7 numerical results for the ρ -meson self-energy are shown. To simplify the discussion, we restrict ourselves to the case $\vec{q} = 0$, i.e. $\Sigma_T = \Sigma_L = \Sigma$. Let us first discuss the imaginary part of the self-energy, $\text{Im } \Sigma$.

The dotted line shows the self-energy in vacuum and is identical to that in Fig. 3 (except that a given energy q_0 in Fig. 7 corresponds to a higher energy q'_0 in Fig. 3, because of the 3-momentum $|\vec{q}'| = 200$ MeV), with the 2-pion threshold at $q^2 = 4m_\pi^2$.

The dashed line shows the self-energy at nuclear saturation density $\varrho_B = \varrho_0$ and zero temperature. The following medium modifications are visible (they have been discussed in detail in Ref. [15]): The threshold disappears, because the ρ -meson can “decay” into two Nh excitations. At higher energies, $q_0 \gtrsim 500$ MeV, the medium contribution to $\text{Im } \Sigma$ is very large, mainly as a result of the “decay” of the ρ -meson into a pion and a transverse Δh excitation ($r = 6$ term, diagram 6f).

The solid line shows the ρ -meson self-energy at density $\varrho_B = \varrho_0$ and temperature $T = 150$ MeV. For a discussion of the differences to the $T = 0$ case, consider Eq. (19), which describes the imaginary part of the $r = 1$ term (the imaginary parts of the other terms have the same structure). The first integral contributes already at $T = 0$, but is enhanced at $T > 0$ by the Bose-factor $1 + f(\omega) + f(q_0 - \omega)$. It describes the “decay”

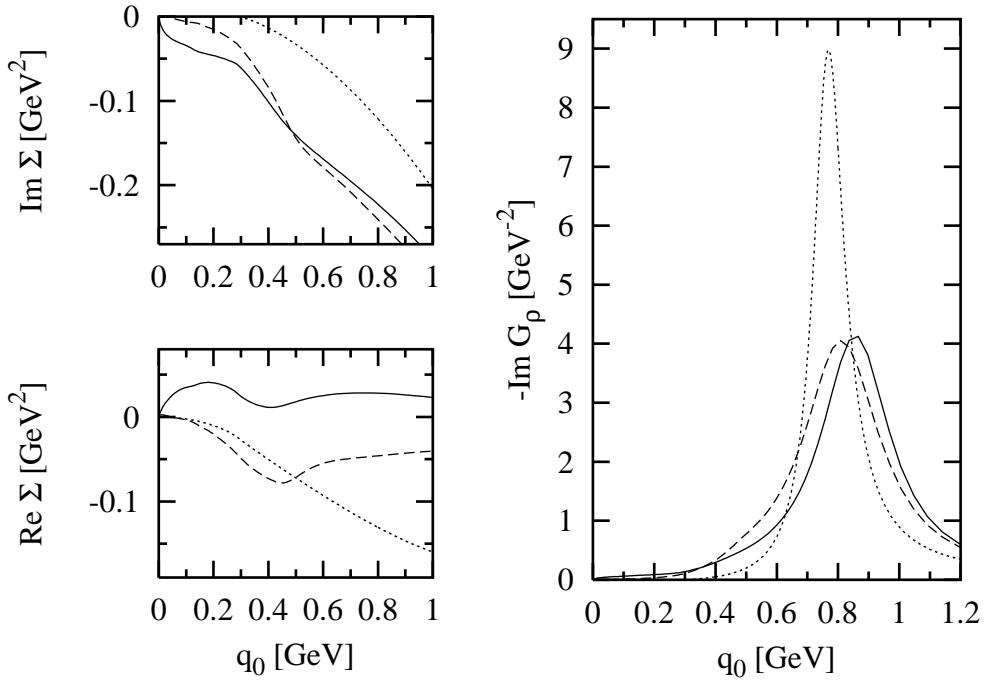


Figure 7: (Left panel) Real and imaginary parts of the ρ -meson self-energy for fixed $|\vec{q}| = 0$ as a function of q_0 in vacuum (dotted lines) and in hadronic matter ($\varrho_B = \varrho_0 = 0.16 \text{ fm}^{-3}$) at temperatures $T = 0$ (dashed lines) and $T = 150 \text{ MeV}$ (solid lines). (Right panel) Corresponding ρ -meson spectral functions.

of the ρ -meson into two in-medium pions with energies ω and $q_0 - \omega$ (Fig. 2c with the free pions replaced by in-medium ones: $\rho \rightarrow \pi_{med} + \pi_{med}$, including processes such as $\rho \rightarrow Nh + \pi$, $\rho \rightarrow \Delta h + \pi$ etc.) and is therefore most important at higher energies, $q_0 \gtrsim 300 \text{ MeV}$. Because of the factor $1 + f(\omega) + f(q_0 - \omega)$ we expected this contribution to increase with temperature, but comparing the two curves in Fig. 7 one sees that it even decreases at energies $q_0 \gtrsim 500 \text{ MeV}$. The reason for this surprising effect is that the medium modifications of the pions become smaller at higher temperatures (see Fig. 4), overcompensating the effect of Bose-enhancement, $1 + f(\omega) + f(q_0 - \omega)$.

At low energies, $q_0 \lesssim 300 \text{ MeV}$, the imaginary part of the self-energy is dominated by the second integral in Eq. (19), which exists only at $T > 0$ because of the factor $f(\omega) - f(q_0 + \omega)$. Therefore $\text{Im } \Sigma$ increases strongly with temperature in this low-energy region, as can be seen in Fig. 7. The corresponding physical process is the “absorption” of the ρ -meson by a thermal pion with energy ω , giving the outgoing pion the energy $q_0 + \omega$ (Fig. 2d with the free pions replaced by in-medium ones: $\rho + \pi_{med} \rightarrow \pi_{med}$). In the absence of baryons, $\varrho_B = 0$, this is possible only for space-like 4-momentum, $q^2 < 0$, i.e. for $q_0 < |\vec{q}|$ (see Section 2). At finite baryon density the situation changes, however, as a consequence of the broadening of the pion spectral function. Even a ρ -meson with 3-momentum $\vec{q} = 0$ can be absorbed by a thermal pion with energy $\omega \gtrsim m_\pi$, if the outgoing “pion” is e.g. a Δh excitation with energy $q_0 + \omega \approx m_\Delta - m_N$. (This process, $\rho + \pi \rightarrow \Delta h$, is of course contained in the class of processes $\rho + \pi_{med} \rightarrow \pi_{med}$.) In this

example the ρ -meson energy must be approximately $m_\Delta - m_N - m_\pi \approx 150$ MeV, but if one considers the Fermi and thermal motion of all participating particles, this process is in principle possible for any ρ -meson energy q_0 .

Comparing the three curves for the real part of the self-energy, $\text{Re } \Sigma$, shown in Fig. 7, we find that both density and temperature increase $\text{Re } \Sigma$ in the region of the ρ -meson pole, shifting it to higher energies. This is evident in the spectral functions, which are also shown in Fig. 7. For the case $\varrho_B = 0$ we have noted this temperature effect already in Section 2 (Fig. 3). It is caused by the real parts of the terms describing the “absorption” of the ρ -meson by a thermal pion (see discussion above). In Fig. 7 this can be inferred from the steep rise of $\text{Re } \Sigma$ in the region where these terms contribute to $\text{Im } \Sigma$, i.e. in the interval $0 < q_0 \lesssim 300$ MeV (in Fig. 3 the corresponding rise of $\text{Re } \Sigma_T$ can be observed in the interval $0 < q_0 < 200$ MeV, whereas $\text{Re } \Sigma_L$ behaves more complicated because of the factor q^2/q_0^2 in Eq. (3)). The imaginary part of these terms itself is almost invisible in the ρ -meson spectral function, because it lies far away from the pole.

5 Dilepton and photon rates

Our original motivation for the investigation of the ρ -meson in hot and dense matter was the description of dilepton production in heavy-ion collisions. Assuming hadronic matter in (local) thermal and chemical equilibrium (temperature T , baryon chemical potential μ_B) and vector meson dominance, the production rate ($R = dN/d^4x$) of e^+e^- pairs with 4-momentum q in the low invariant mass region ($M = \sqrt{q^2} < 1$ GeV) is given by [8]

$$\frac{dR_{e^+e^-}}{d^4q} = \frac{\alpha^2}{3\pi^3 M^2} \frac{1}{e^{q_0/T} - 1} \frac{(m_\rho^{(0)})^4}{g^2} g_{\mu\nu} \text{Im } G_\rho^{\mu\nu}(q_0, \vec{q}; \varrho_B, T), \quad (21)$$

where $\alpha = e^2/(4\pi) = 1/137$. In the derivation of this expression the electron mass has been neglected. Eq. (21) can be rewritten in terms of the longitudinal and transverse propagators as

$$g_{\mu\nu} \text{Im } G_\rho^{\mu\nu} = -2 \text{Im } G_{\rho T} - \text{Im } G_{\rho L}. \quad (22)$$

Results for the dilepton rate as a function of M , i.e. integrated over \vec{q} , are displayed in Fig. 8. It should be kept in mind, however, that for a realistic description also the self-energy contributions $\Sigma_{\rho B}$ (Fig. 1b) and $\Sigma_{\rho M}$ (Fig. 1c) have to be included, which are missing here. The solid line shows the rate obtained with a ρ -meson propagator containing the $\Sigma_{\rho\pi\pi}$ self-energy as described in the previous sections. The dashed line has been calculated using the zero-temperature ρ -meson propagator, i.e. $G_\rho(q_0, \vec{q}; \varrho_B, T)$ in Eq. (21) has been replaced by $G_\rho(q_0, \vec{q}; \varrho_B, T = 0)$. This is the approximation that has been employed e.g. in Ref. [15]. For the dotted line the ρ -meson propagator in vacuum has been used.

Compared with the dotted curve, both dilepton spectra obtained with spectral functions calculated at $\varrho_B = \varrho_0$ (dashed and solid lines) are strongly enhanced in the invariant mass region below 600 MeV, and the peak at the ρ -meson mass, $600 \text{ MeV} \lesssim M \lesssim 800$ MeV, has disappeared. This is a consequence of the broadening of the spectral function, which is mainly an effect of baryon density. Contrary to the strong density effect, the

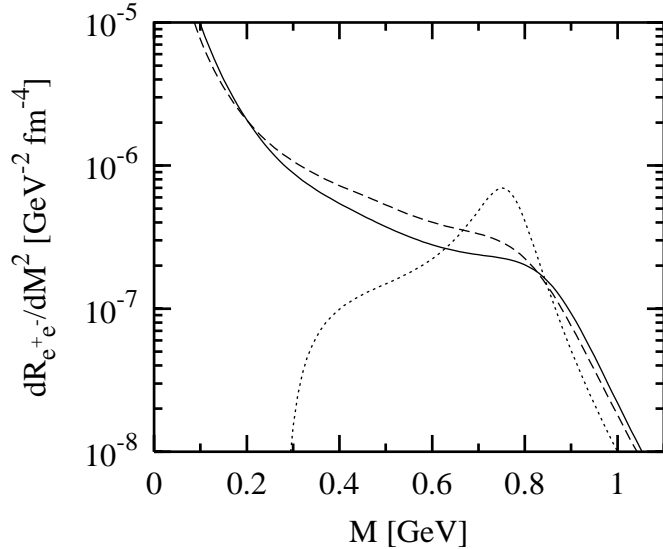


Figure 8: Dilepton production rate $dR_{e^+e^-}/dM^2$ at $\varrho_B = \varrho_0$ and $T = 150$ MeV (solid line) and results obtained with different approximations to $G_\rho(\varrho_B, T)$: $G_\rho(\varrho_B, T = 0)$ (dashed line) and $G_\rho(\varrho_B = 0, T = 0)$ (dotted line).

pure temperature effect, i.e. the difference between the dashed and the solid curve, is less than a factor 1.5. As the maximum of the ρ meson spectral function is shifted to higher M at finite temperature, the dilepton rate is reduced for $200 \text{ MeV} \lesssim M \lesssim 800 \text{ MeV}$, while it is enhanced above 800 MeV.

Besides dilepton pairs, also direct real photons (i.e. real photons produced inside the fireball) can be used as probes for the hot and dense phase of the fireball in heavy-ion experiments. If we make the same assumptions as in the derivation of Eq. (21), the rate for direct real photon emission is given by [21]

$$q_0 \frac{dR_\gamma}{d^3q} = \frac{\alpha}{2\pi^2} \frac{1}{e^{q_0/T} - 1} \frac{(m_\rho^{(0)})^4}{g^2} g_{\mu\nu} \text{Im } G_\rho^{\mu\nu}(q_0, \vec{q}; \varrho_B, T), \quad (23)$$

where $q_0 = |\vec{q}|$ is the energy of a photon with momentum \vec{q} . In this case the longitudinal propagator $G_\rho L$ in the r.h.s. of Eq. (22) vanishes.

Numerical results are shown in Fig. 9. Again the solid line represents the full calculation, while for the dashed line $G_\rho(q_0, \vec{q}; \varrho_B, T)$ in Eq. (23) has been replaced by the zero-temperature propagator, $G_\rho(q_0, \vec{q}; \varrho_B, T = 0)$. The enhancement of the solid curve below 350 MeV is a consequence of the imaginary part of the “absorption” terms discussed at the end of Section 4, which in the context of photon emission correspond to processes such as $\pi_{med} \rightarrow \pi_{med} + \rho \rightarrow \pi_{med} + \gamma$, e.g. $\Delta h \rightarrow \pi + \rho \rightarrow \pi + \gamma$. At higher energies, $q_0 \gtrsim 350$ MeV, the rate is dominated by the “decay” terms, corresponding to annihilation processes such as $\pi_{med} + \pi_{med} \rightarrow \rho \rightarrow \gamma$, e.g. $\Delta h + \pi \rightarrow \rho \rightarrow \gamma$. In this range the photon rate obtained with the finite-temperature ρ -meson propagator is strongly reduced (to 60% of the dashed curve for $q_0 \gtrsim 600$ MeV) because of the smaller medium modifications of the pion propagator.

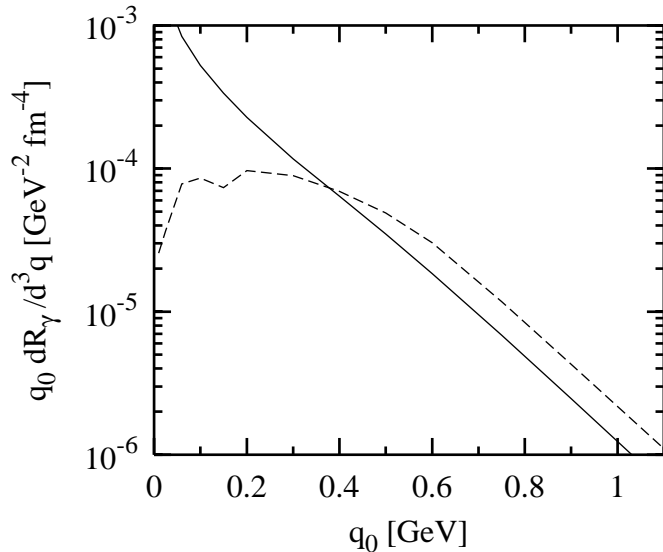


Figure 9: Direct real photon emission rate $q_0 dR_\gamma/d^3q$ at $\varrho_B = \varrho_0$ and $T = 150$ MeV within the full model (solid line) and with $G_\rho(\varrho_B, T)$ replaced by $G_\rho(\varrho_B, T = 0)$ (dashed line).

We stress again that our results are not predictions for the total rates, but only for the contribution $\Sigma_{\rho\pi\pi}$. As a rough estimate of the relevance of this contribution we recall that to leading order in ϱ_B and T the baryon-density contribution to the total photon emission rate can be related to the photoabsorption cross-section of the nucleon [21]. In fact, our dashed curve in Fig. 9 is proportional to the “background” of the photoabsorption cross section for nuclear matter [15, 16], except for a factor $q_0/(e^{q_0/T} - 1)$. As shown in Ref. [16], the background amounts to $\approx 20\%$ of the total cross-section in the Delta region and more at higher energies. Although, in general, one cannot simply add the different contributions $\Sigma_{\rho\pi\pi}$, $\Sigma_{\rho B}$ and $\Sigma_{\rho M}$, because they appear in the denominator of the ρ -meson propagator, it is reasonable to assume that the $\Sigma_{\rho\pi\pi}$ contribution to the total photon and dilepton production rates is also of the order of 20% and therefore should be treated correctly.

6 Summary and conclusions

In a previous article [15] we have extended the models from Refs. [8, 9], describing the modifications of the ρ -meson through the in-medium pion propagator in cold nuclear matter, to finite 3-momentum of the ρ -meson. In the present work we have also included finite-temperature effects by evaluating both, the pion and ρ -meson self-energy diagrams within the imaginary-time formalism.

For fixed baryon density ϱ_B , the medium modifications of the pions are reduced at finite temperature because the nucleon density ϱ_N becomes smaller and Δh excitations are additionally suppressed by Pauli blocking of Delta states.

When evaluating the ρ -meson self-energy diagrams with in-medium pion propagators, care must be taken to preserve gauge invariance, since the $\rho\pi\pi$ and $\rho\rho\pi\pi$ vertex functions are related to the pion propagator by Ward-Takahashi identities. Therefore vertex

corrections have to be included.

Because of the soft form factor at the πNN and $\pi N\Delta$ vertices the medium modifications of the self-energy contribution $\Sigma_{\rho\pi\pi}$ are smaller than those found in our previous article, but still this contribution leads to significant changes of the ρ -meson spectral function already at nuclear saturation density, $\varrho_B = \varrho_0$. Let us summarize the most important effects: First, the width of the ρ -meson is increased. This is mainly a density effect and, for not too small densities, almost independent of temperature. Second, the maximum of the ρ -meson spectral function, i.e. the ρ -meson “mass”, is slightly shifted upwards in the medium. This shift increases with both, density and temperature. Third, the two-pion threshold disappears. At very low energies, the imaginary part of the ρ -meson self-energy, and therefore also the spectral function, is strongly enhanced at finite temperature.

Over a wide range the dilepton and photon production rates obtained with the finite-temperature spectral function are reduced compared with those obtained with the zero-temperature spectral function. This is a consequence of the smaller medium modifications of the pion propagators at finite T and the upward shift of the ρ -meson pole mass. Only in the real photon emission rates at low energies the temperature effects lead to an enhancement of the rate. However, these changes are not dramatic, since the contribution of $\Sigma_{\rho\pi\pi}$ is less important than that of $\Sigma_{\rho B}$, which we have not considered here [14].

In some respects the model could be further improved. First, for the description of the pion in nuclear matter also higher resonances beyond the $\Delta(1232)$ should be included. Probably this would at least partially compensate the suppression of the medium modifications of the pion propagator at finite temperature (see footnote in Section 3). Second, for the case $T > 0$ but $\varrho_B = 0$, it has been shown that in a consistent treatment of ρ - and a_1 -mesons, respecting chiral symmetry, finite temperature mainly results in a mixing of vector and axial-vector correlators, i.e. ρ - and a_1 -meson propagators [22]. To relate the measured dilepton spectra to potential signals of chiral symmetry restoration it is mandated to study the medium modifications of ρ - and a_1 -mesons within a chiral symmetric model also at $\varrho_B \neq 0$. Work in this direction is in progress.

Acknowledgements

We thank R. Rapp for valuable discussions. This work was supported in part by GSI, BMBF and NSF grant NSFPHY98-00978.

A Explicit expressions and definitions

In Section 4 only the structure of the formula for the spatial components of the ρ -meson self-energy has been given (Eqs. (11) and (16)). The explicit expression reads

$$\begin{aligned}
\Sigma_{ij}(q_0, \vec{q}) = & \frac{g^2}{4} \int \frac{d^3 k}{(2\pi)^3} \left((2k + q)_i (2k + q)_j I_1(q_0, \vec{q}, \vec{k}) \right. \\
& + 4 \frac{(k_i(\Lambda^2 - \vec{k}^2) - q_i \vec{k}^2)(2k + q)_j}{\Lambda^2 + (\vec{k} + \vec{q})^2} I_2(q_0, \vec{q}, \vec{k}) \\
& + 2 \frac{(k_i(\Lambda^2 - \vec{k}^2) - q_i \vec{k}^2)(k_j(\Lambda^2 - \vec{k}^2) - q_j \vec{k}^2)}{\vec{k}^2(\Lambda^2 + (\vec{k} + \vec{q})^2)^2} I_3(q_0, \vec{q}, \vec{k}) \\
& + 2 \frac{(k_i(\Lambda^2 - \vec{k}^2) - q_i \vec{k}^2)(k_j(\Lambda^2 - (\vec{k} + \vec{q})^2) + q_j \Lambda^2)}{(\Lambda^2 + (\vec{k} + \vec{q})^2)(\Lambda^2 + \vec{k}^2)} I_4(q_0, \vec{q}, \vec{k}) \\
& + 2\delta_{ij} J_5(\vec{k}) \\
& + 2 \frac{(\Lambda^2 + \vec{k}^2)^2}{(\Lambda^2 + (\vec{k} + \vec{q})^2)^2} \left(\delta_{ij} - \frac{k_i k_j}{\vec{k}^2} \right) I_6(q_0, \vec{q}, \vec{k}) \\
& \left. - 4 \left(\frac{\vec{k}^2 \delta_{ij}}{\Lambda^2 + \vec{k}^2} + \frac{(2k + q)_i (k_j(\Lambda^2 - \vec{k}^2) - q_j \vec{k}^2)}{(\Lambda^2 + (\vec{k} + \vec{q})^2)(\Lambda^2 + \vec{k}^2)} \right) J_7(\vec{k}) \right) \\
& + (i \longleftrightarrow j) . \tag{24}
\end{aligned}$$

The retarded functions I_r are given by analytical continuation of the corresponding imaginary-time functions J_r to the real axis according to Eq. (17). The functions J_1 to J_7 are defined as follows:

$$J_1(\omega_n, \vec{q}, \vec{k}) = -2T \sum_{m \text{ even}} \mathcal{G}_\pi(\omega_m, \vec{k}) \mathcal{G}_\pi(\omega_{m+n}, \vec{k} + \vec{q}) , \tag{25}$$

$$J_2(\omega_n, \vec{q}, \vec{k}) = -2T \sum_{m \text{ even}} \Pi(\omega_m, \vec{k}) \mathcal{G}_\pi(\omega_m, \vec{k}) \mathcal{G}_\pi(\omega_{m+n}, \vec{k} + \vec{q}) , \tag{26}$$

$$J_3(\omega_n, \vec{q}, \vec{k}) = -2T \sum_{m \text{ even}} \Pi_L(\omega_m, \vec{k}) \mathcal{G}_\pi(\omega_{m+n}, \vec{k} + \vec{q}) , \tag{27}$$

$$\begin{aligned}
J_4(\omega_n, \vec{q}, \vec{k}) = & -2T \sum_{m \text{ even}} \Pi(\omega_m, \vec{k}) \mathcal{G}_\pi(\omega_m, \vec{k}) \\
& \times \Pi(\omega_{m+n}, \vec{k} + \vec{q}) \mathcal{G}_\pi(\omega_{m+n}, \vec{k} + \vec{q}) , \tag{28}
\end{aligned}$$

$$J_5(\vec{k}) = -2T \sum_{m \text{ even}} \mathcal{G}_\pi(\omega_m, \vec{k}) , \tag{29}$$

$$J_6(\omega_n, \vec{q}, \vec{k}) = -2T \sum_{m \text{ even}} \Pi(\omega_m, \vec{k}) \mathcal{G}_\pi(\omega_{m+n}, \vec{k} + \vec{q}) , \tag{30}$$

$$J_7(\vec{k}) = -2T \sum_{m \text{ even}} \Pi(\omega_m, \vec{k}) \mathcal{G}_\pi(\omega_m, \vec{k}) . \tag{31}$$

The imaginary-time pion self-energy Π and propagator \mathcal{G}_π are related to the corre-

sponding retarded functions Π and G_π by their Lehmann representations

$$\Pi(\omega_m, \vec{k}) = -\frac{1}{\pi} \int d\omega \frac{\text{Im } \Pi(\omega, \vec{k})}{i\omega_m - \omega}, \quad G_\pi(\omega_m, \vec{k}) = -\frac{1}{\pi} \int d\omega \frac{\text{Im } G_\pi(\omega, \vec{k})}{i\omega_m - \omega}. \quad (32)$$

As a consequence, such representations exist also for ΠG_π and Π_L , which are combinations of these functions. The “longitudinal spin-isospin response function” Π_L is defined by

$$\begin{aligned} \Pi_L(k_0, \vec{k}) &= \Pi(k_0, \vec{k}) + \Pi(k_0, \vec{k}) \vec{k}^2 G_\pi(k_0, \vec{k}) \Pi(k_0, \vec{k}) \\ &= (k^2 - m_\pi^2) \Pi(k_0, \vec{k}) G_\pi(k_0, \vec{k}). \end{aligned} \quad (33)$$

References

- [1] E.V. Shuryak, Phys. Lett. B 78 (1979) 150.
- [2] J.J. Sakurai, Ann. Phys. 11 (1960) 1.
- [3] N.M. Kroll, T.D. Lee and B. Zumino, Phys. Rev. 157 (1967) 1376.
- [4] R. Rapp and J. Wambach, preprint hep-ph/9907502, to be published in Adv. Nucl. Phys.
- [5] T. Ericson and W. Weise, Pions and Nuclei (Oxford University Press, New York, 1988).
- [6] C. Gale and J. Kapusta, Phys. Rev. C 35 (1987) 2107.
- [7] C.L. Korpa and S. Pratt, Phys. Rev. Lett. 64 (1990) 1502.
- [8] G. Chanfray and P. Schuck, Nucl. Phys. A 555 (1993) 329.
- [9] M. Herrmann, B. Friman and W. Nörenberg, Nucl. Phys. A 560 (1993) 411; M. Herrmann, PhD thesis, Darmstadt 1992 (GSI-Report 92-10).
- [10] B. Friman and H.J. Pirner, Nucl. Phys. A 617 (1997) 496.
- [11] W. Peters, M. Post, H. Lenske, S. Leupold and U. Mosel, Nucl. Phys. A 632 (1998) 109.
- [12] G. Agakichiev et al., CERES collaboration, Phys. Rev. Lett. 75 (1995) 1272; P. Wurm for the CERES collaboration, Nucl. Phys. A 590 (1995) 103c. G. Agakichiev et al., CERES collaboration, Phys. Lett. B 422 (1998) 405.
- [13] R. Rapp, G. Chanfray and J. Wambach, Nucl. Phys. A 617 (1997) 472.
- [14] R. Rapp and J. Wambach, preprint hep-ph/9907502.
- [15] M. Urban, M. Buballa, R. Rapp and J. Wambach, Nucl. Phys. A 641 (1998) 433.
- [16] R. Rapp, M. Urban, M. Buballa and J. Wambach, Phys. Lett. B 417 (1998) 1.
- [17] A.L. Fetter and J.D. Walecka, Quantum Theory of many-particle systems (McGraw-Hill, New York, 1971).
- [18] C. Gale and J.I. Kapusta, Nucl.Phys. B 357 (1991) 65.
- [19] A.B. Migdal, Rev. Mod. Phys. 50 (1978) 107.
- [20] J.F. Mathiot, Nucl. Phys. A 412 (1984) 201.
- [21] J.V. Steele, H. Yamagishi and I. Zahed, Phys. Rev. D 56 (1997) 5605.
- [22] M. Dey, V.L. Eletsky and B.L. Ioffe, Phys. Lett. B 252 (1990) 620, V.L. Eletsky and B.L. Ioffe, Phys. Rev. D 51 (1995) 2371.